Time calibration for the SciFi Tracker at SND@LHC using DESY testbeam data

Jennifer Maria Frieden
jennifer.frieden@epfl.ch

April 23, 2020

Professor:
Prof. Dr. Olivier Schneider

Supervisors:
Dr. Guido Haefeli
Dr. Ana Barbara Rodrigues Cavalcante
Doctoral Assistant Carina Trippl

Abstract

A Scintillating Fibre Tracker with timing information was developed by LPHE at EPFL. To evaluate its timing and tracking performance, a test beam campaign was organized at DESY in October 2019. By using this data, the different time delays and offsets that could influence the time resolution measurement are quantified. Besides, several algorithms to measure the track time in each event were developed. The main goal of this project is to use the time information of the track in the time calibration of the SciFi Tracker leading to a time resolution of about 250ps, a $\sqrt{2}$ factor better than the previous result of $\sigma_{CTR} = 350$ps. This measurement procedure is also verified by introducing artificially calibration errors that are recovered after using the track information.

Contents

1 Introduction

The Standard Model of particle physics (SM) describes known phenomena with great precision. However, it does not explain for example the existence of dark matter or the baryon-antibaryon asymmetry in the Universe [1]. A new experiment called SND@LHC is going to exploit new physics by studying neutrino flavours, and is thus searching for dark matter particles. A group of the laboratory of high energy physics (LPHE) of EPFL is involved with the development and design of a Scintillating Fibre Tracker (SciFi) with timing information that is part of this detector.

The detector has to be very well calibrated to ensure good time and spatial resolution before instalment. For this, data taken during a testbeam at DESY is studied. In particular, the focus of the project is placed on an alternative method to enhance the time resolution using the track information. The determination of the time offsets and delays is the key to calibrate the detector as best as possible.

2 SND@LHC

The Scattering Neutrino Detector (SND) is planned to be installed at the Large Hadron Collider (LHC) at CERN, in May 2021. SND is expected to provide new information about different phenomena in neutrino physics, with a special focus on τ neutrinos. The desired particles all have the property to interact weakly. Therefore, the cavern TI18 close to the ATLAS collision point has been chosen for the instalment, as the detector is shielded from heavy particles, but is still close enough to get a a filtered jet of particles [1].

Neutrinos are neutral particles, which have to be detected indirectly through ionisation of matter. In fact, through lepton flavour number conservation in weak interactions, a neutrino always decays into its conjugated lepton as product. The leptons $e^{\pm}$, $\mu^{\pm}$ and $\tau^{\pm}$ are all charged and their detection in SND is a strong indication that they are originating from a decay of a neutrino.

The configuration of the SND detector is shown in figure 1. The SND detector is composed of two main regions: the Target region and the muon system. Their main components and their applications are discussed below.

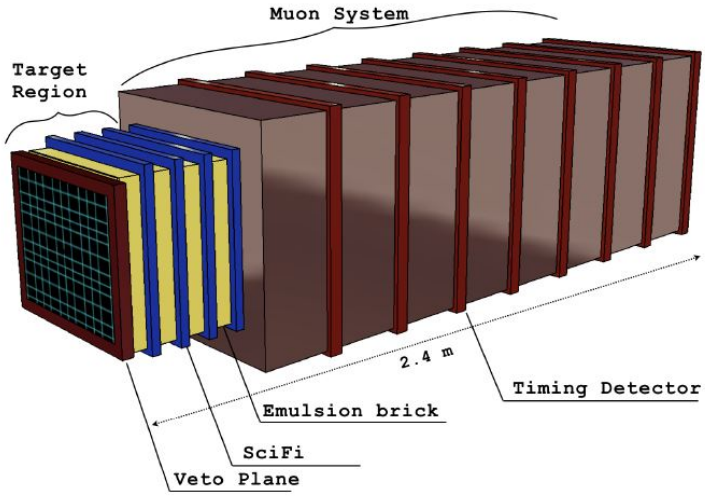

FIGURE 1: *Schematic view of the Neutron Scattering Detector [1].*

- **Veto plane**

  The first part of the target region consist of a Veto plane, which acts as a first scan over the particles, classifying them as possible candidates or other. It vetoes charged particles, in particular muons which are coming from background sources, such as cosmic rays or directly from ATLAS. The particle of interest of the experiment are the charged leptons that are created in the detector by neutrino decay.

- **Emulsion Cloud Chambers**

  One of the main components of the target region consist of Emulsion Cloud Chambers (ECC), which are nuclear emulsion films interleaved with blocks of high Z material. An ECC is generally used for tracking the particles passing through the block of matter, with a spatial resolution up to micrometric range. They are used in SND for their high spatial resolution. The data of the emulsion films cannot be collected instantaneously as they do not have an electric readout system.

- **SciFi planes**

  The second main component of the target region are the hybrid SciFi layers. After each emulsion block, a hybrid SciFi plane is needed for complete information. Those planes give electronic information of the time and position measurement of the arriving hits in real time. In total there are four such planes installed in the target region.

- **Muon chambers**

  The last and biggest part of SND is a muon detection chamber. It is composed of iron slabs and scintillating planes. The iron slabs are acting as calorimeter, whereas the scintillator planes are the timing detector in the muon system. Muonic flavoured neutrinos will decay in the detector and produce muons, which are finally detected in the muon chambers. The muon system works together with the Veto plane in order to separate the muons that have been produced by beta decay in the emulsion and the ones coming from ATLAS or other background sources.

The time alignement of the SND detector is synchronised with the LHC machine, and it uses a Time and Trigger control (TTC) system [2]. Beside the time alignement, muon tracks are also available for calibration. Using muon tracks for time calibration for the SciFi layers in SND experiment would be perfect if this type of calibration is efficient. This would allow to get a precise calibration, and therefore improve the time resolution of the SciFi Tracker.

3 Scintillating Fibre Tracker

The LPHE group at EPFL has been involved in the design and construction of particle detectors using the scintillating fibre technology. Henceforth, the scintillating fibre (SciFi) tracker used in the testbeam campaign on DESY in October 2019 is described in detail (see figure 2).

The SciFi tracker consists of two main components: (i) Scintillating fibres as the active detector material and (ii) readout system using Silicon Photomultipliers (SiPM).

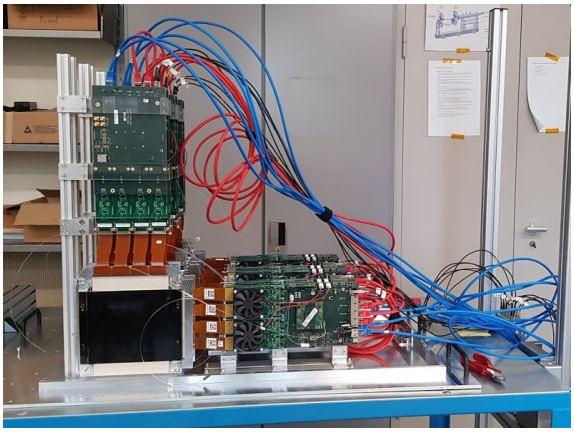

FIGURE 2: *An example of a SciFi tracker used during a data taking campaign at DESY. [3].*

3.1 Scintillating fibres

A fibre mat consists of several staggered-layers of scintillating fibre forming a squared plane of 133mm side length. Two fibre mats, one perpendicular to the other, form the X and Y direction of a plane. In a scintillating fibre, light is produced from the energy deposit of crossing charged particles, and transported over its length to the photodetectors situated at one end of the fibre mat. The SciFi Tracker setup used for the data acquisition consists of six fibre planes and twelve boards. Each board is reading out the signal collected by 512 SiPM channels.

The fibre is made of a polymer core, which is doped with a primary and a secondary scintillator. The scintillation follows the steps described in figure 3. The charged particle crossing the fibre excites the molecules of the polymer core fibre, which deposits energy. The energy is rapidly transferred to the primary scintillator by Förster transfer, which is a non-radiative dipole-dipole process. The primary scintillator de-excites almost instantaneously into a UV photon, which propagates to the secondary scintillator. The last one acts as a wavelength shifter and emits photons that are in the blue wavelength range, where the fibre is more transparent.

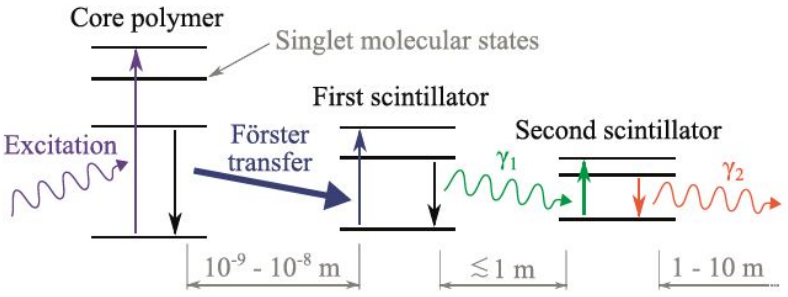

FIGURE 3: *Scintillation process in the polymer core of the fibre doped with a primary and a secondary scintillator [4].*

3.2 Silicon Photomultipliers

A Silicon Photomultiplier (SiPM) is an array of Avalanche Photodiodes (APDs). The light produced in the fibre is transported towards the detector, where it is readout and converted into an electric signal. The APD can be visualised as a pixel with an area of 57.5 x 62.5 μm^2, which is composed of an active area, where the photon is detected and processed, and a dead

area (see the left graph of figure 4). The APDs are connected in parallel to each other, and are operating in Geiger-Müller mode. The photon hitting the active area of the APD, creates charge carriers in the silicon layer. The doped silicon layers are adjusted such that a high electric field is obtained, which will accelerate the created charge carriers, create secondary ionisation and start avalanches. In order to obtain a high electric field for the avalanches, the applied voltage has to be above the break-down voltage V_{BD}, where the ionisation of the holes can occur. Therefore, the relevant voltage for a SiPM operation is the overvoltage, which is defined by $\Delta V = V_{bias} - V_{BD}$, where V_{bias} is the applied bias voltage.

On the left hand-side of figure 4, the configuration of the SiPM is shown. It is separated into 128 readout channels, where each of them contains 104 pixels operated in Geiger-Müller mode. The 128-channel module is then separated into two 64-channel silicon dies with a gap of 220μm.

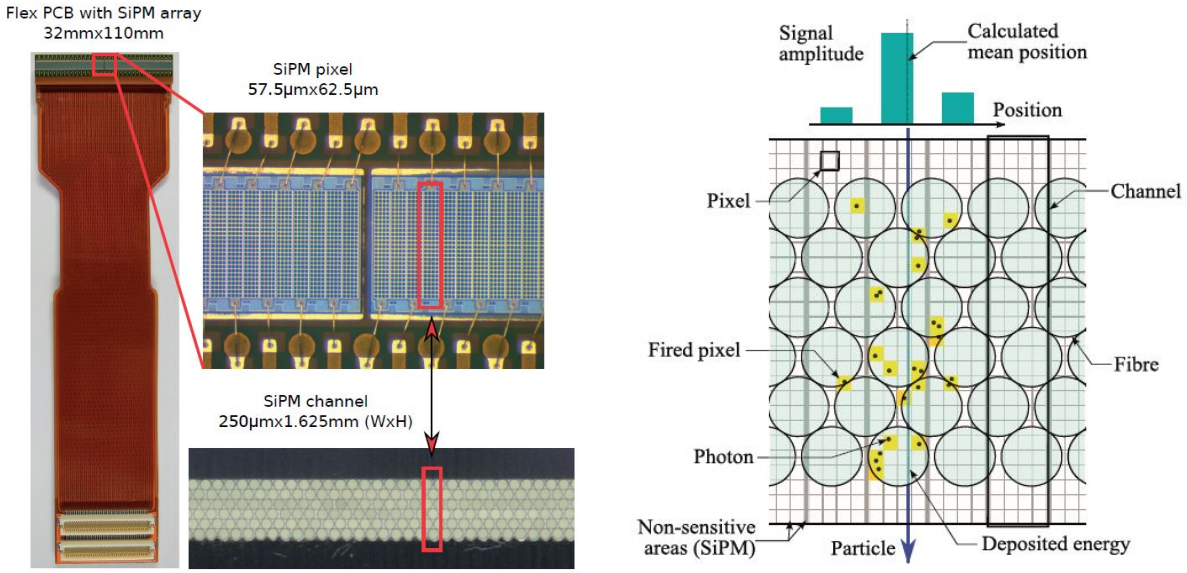

FIGURE 4: *On the left: The SiPM array mounted on a flex PCB is shown on the left and a microscopic view on the right of the channels can be distinguished, as well as a the pixel [5]. On the right graph: A schematic view of the multichannel readout is shown [4].*

On the right hand-side of figure 4, a particle crossing the fibre mat is producing light in more than one fibre, and therefore, the signal is produced in more than one SiPM channel. A cluster is defined as all the channels involved in the multichannel readout of one hit and it has a typical size of 2-3 channels.

3.3 STiC chips

The STiC chip is an analog front end, a built-in time to digital converter and a digital part for configuration and data transmission. The STiC is reading out either even or odd channels of the SiPM. It therefore reads out 64 channels, separated into two Phase Lock Loops (PLLs), circuits of 32 channels each. They are responsible for the fine time counting.

In figure 5, the typical signal of a SiPM is shown. On this pulse, three different thresholds are required for the signal readout process of the STiCs. The energy threshold (ETH), is requiring a large enough voltage of the pulse, while the timing threshold (TTH) measures the rising and the falling edge of the pulse. The combination of both TTH and ETH is the Time Over Threshold (TOT), which is the main requirement of the processing of the signal [6].

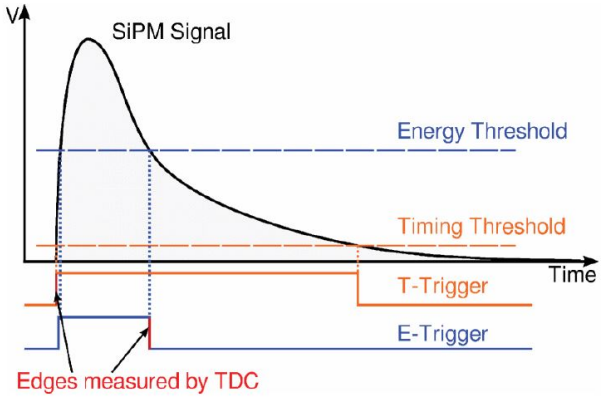

FIGURE 5: *Typical signal emitted by the SiPM and the different threshold in the readout process of the STiCs [4].*

3.4 The Board

The board consist of an electronic card which links all the Data Aquisition (DAQ) systems, with the readout components mentioned above. A DAQ board contains a Field Programmable Gate Array (FPGA), an ARM (the CPU) and eight STiCs reading the signal of the four SiPMs. The main function of the FPGA is to acquire external trigger information and send clocks and resets to the STiCs. The FPGA also RAM stores all the events, while the ARM is reading the data and sending it to a local server [6]. The setup of a board, with its STiCs and SiPMs is shown in figure 6.

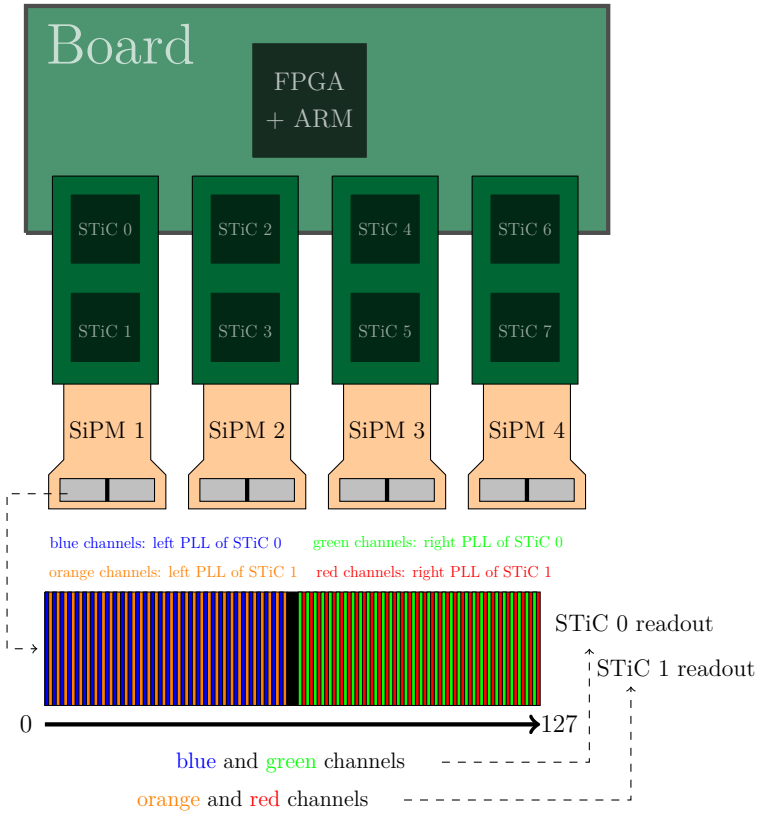

FIGURE 6: *Board configuration, with the STiCs and the SiPMs.*

4 DESY Testbeam

The data used for the analysis has been collected in October 2019 at the *Deutsches Elektronen synchrotron* (DESY) in Hamburg, more precisely in the testbeam area of DESY II. The beam in this area consists of electrons, which can reach energies up to 6 GeV.

In order to take reasonable data, the detector has to be calibrated, means that for this setup, the channels, as well as the boards are adjusted on an equal base for the measurement.

- **Channel time calibration**

  The channel calibration is done by light injection using a Vertical-Cavity Surface-Emitting Laser (VCSEL) mounted on each board itself. The laser illuminates a plastic optical fibre (POF) that is scratched in the injection region, where it illuminates all the 512 channels of the board. The setup for the channel time calibration is shown in figure 7. For each channel, the time difference of the laser signal and the reception of the light is measured and called the channel time offset.

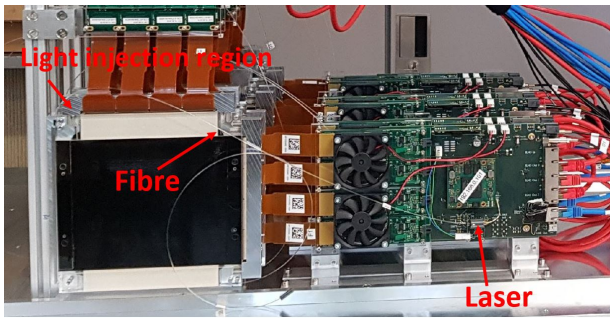

FIGURE 7: *A DAQ board connected to a fibre mat, where the laser light injection calibration through a plastic optical fibre is highlighted [3].*

- **Board time calibration**

  In figure 8, the arrangement of the boards in the z direction is observed. The distance between the first and the last board is 350 mm. The board time calibration has to compensate for this distance, as well as for the length of the cables. This calibration was measured with a trigger system using cosmic rays. The trigger system is made of two scintillator, each coupled to a Photomultiplier Tube (PMT). One small scintillator is put on the top, just in front of the first fibre mat, and the larger one is placed on the bottom, after the last fibre plane. This size difference is due to the angular dispersion of the cosmic rays. Therefore, only full tracks are selected for the calibration, which therefore mainly consist of muons. The time difference between the hit time in the board and the trigger time is measured and is called the board time offset.

FIGURE 8: *The SciFi tracker setup, with the boards separated spatially in the z direction [3].*

The channel time calibration has to be done before each measurement. Different runs have been performed at the DESY testbeam, with different conditions. Overvoltage scans were performed between 4-6 V, where it has been observed that the ideal overvoltage is 5V. Furthermore, to ensure uniformity over the detector, the beam was pointed at different positions of the fibre mat. In the figure 9, the four different positions used, as well as the coordinate system of the fibre mat are displayed. Moreover, lead plates were installed to take data with showers. Lastly, runs in combination with emulsion bricks were performed. All the different measurement, with all the details, are referred in the Twiki [3].

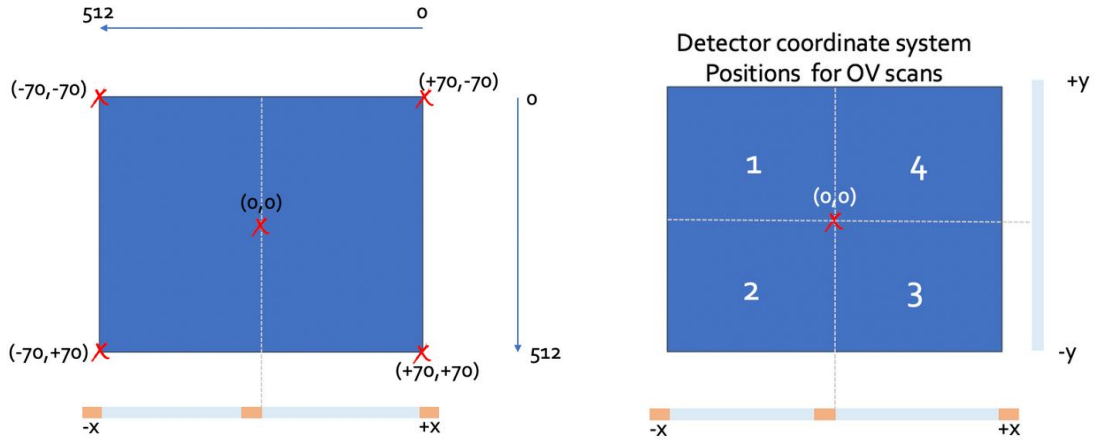

FIGURE 9: *On the left: Schematic view of the coordinates on a fibre mat, coupled to the channels. On the right: Schematic view of the four different positions used of the beam [3].*

5 Time resolution analysis

The aim of this project is to evaluate and minimise the time resolution of the SciFi detector by improving the time calibration. The expected time resolution is of the order of magnitude of a few hundreds of ps. The calibration consists on determining the different time offsets and delays of the system and compensate for these.

For the analysis, ideal runs from DESY testbeam are used, to have the best estimation as possible of the time offsets. The runs 1213, 1214, 1215 and 1216 have been used in the data analysis with an overvoltage set at 5V and with no interlaying material. They differ by the quadrant position the beam hits the SciFi tracker (see figure 9).

5.1 Channel time offsets

In order to evaluate the time calibration for the channels, an analysis of the measured channel time offset is performed in this first subsection. Exceptionally, all the runs collected at DESY are used for this part of the analysis.

Runs selection

Firstly, a selection is done choosing all the runs which have an available calibration file. The selection requirement is that it contains no dead channels. A summary of the qualification of the runs is exported in a text file (see extract in the table in appendix A). The selection is in agreement with the indications of the Twiki [3].

Mean channel offset per STiC, PLL, and board

The stability of the channel time offset is evaluated over all selected runs with good calibration for all channels and all boards by extracting the mean time offset as well as its standard deviation. In order to obtain a qualitative analysis, the values of the offsets are classified into STiCs and PLLs. Figure 10 shows the mean channel time offset for board 3 (see in the appendix B for the other boards).

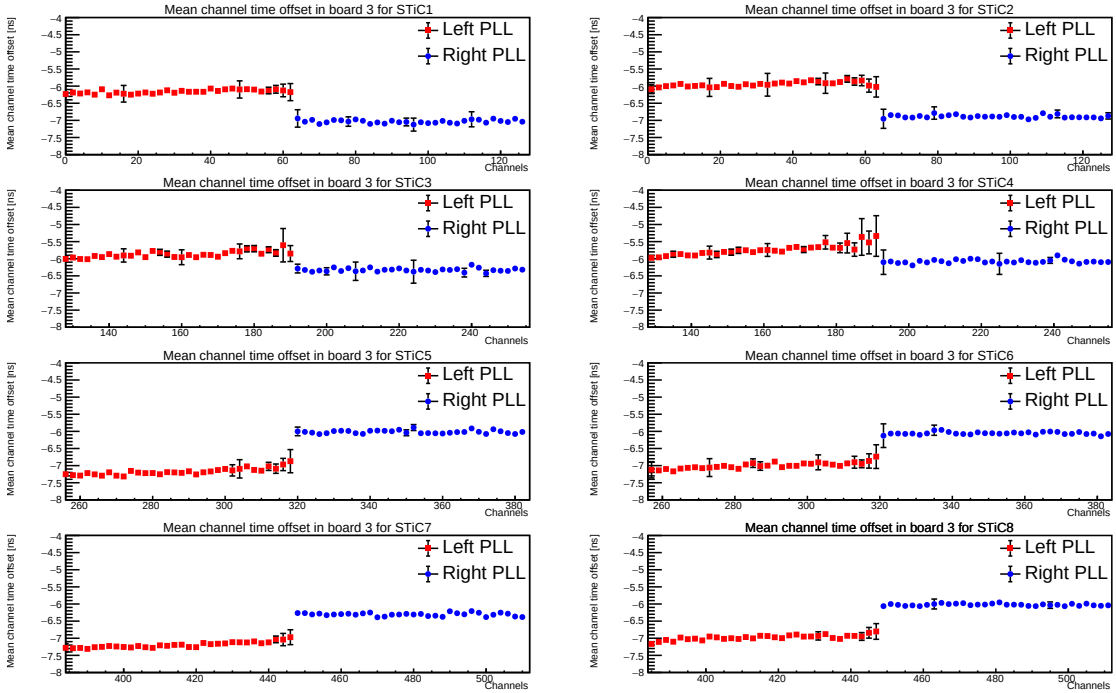

FIGURE 10: *Mean channel offsets per STiC and PLL in board 3.*

Reproducibility

In figure 10, it is noticeable that some channels have a larger deviation (for example for STiC 4, channels 188-194). A typical histogram of the channel offset of a single channel is shown in figure 11, where the main peak is clearly distinguishable, however there are some entries at 1.84ns far from it, which are coming from the calibration and some entries around -7.85ns, which correspond to faulty calibration runs. Those entries which are far from the main peak are responsible for increasing considerably the standard deviation, which explains the larger error bar for this channel in figure 10.

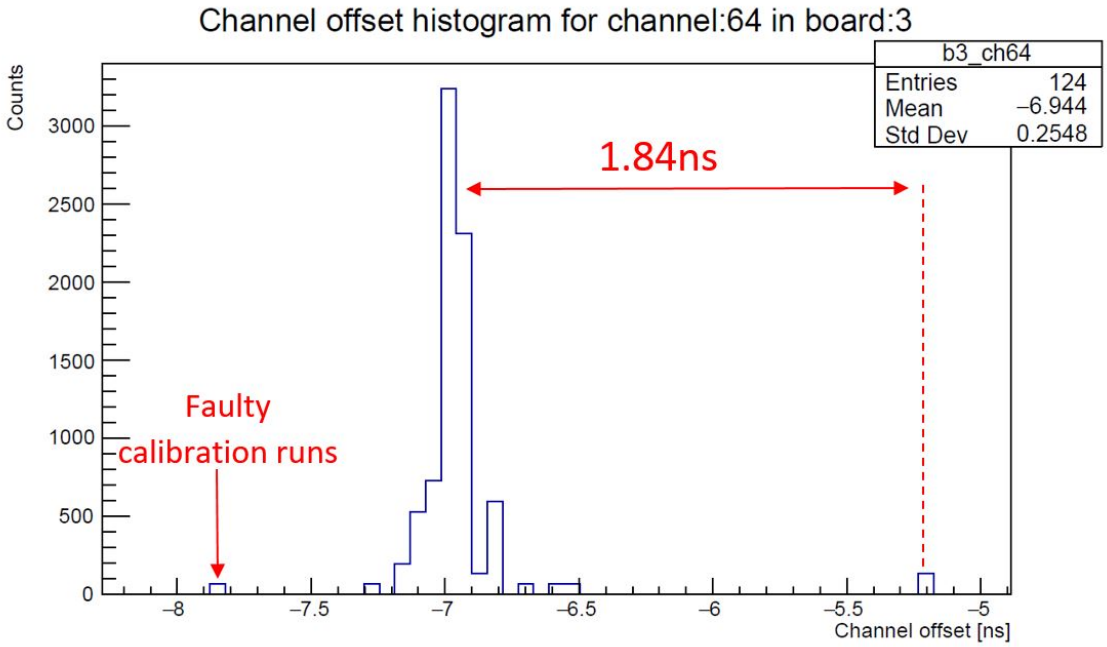

FIGURE 11: *Channel offset distribution for the channel 64 in board 3.*

An algorithm classifies all the histograms into different categories and table 1 shows the percentage of the channel in each category and board. The numbers in table 1 show that the channel offsets were measured in a consistent way and that most of them describe a clean main peak with or without noise. However, a non negligible amount of channels present some entries shifted by ±1.84ns, because of a known bug in the STiC chip. This problem can be solved by changing the chip.

In order to simplify the classification, the following codes are used to distinguish the type of histogram of the channel offset:

- **0 :** Describes a clean peak
- **0.1 :** Describes a clear peak, but with some entries further than 0.25ns from the maximum of the main peak
- **1 :** Describes a clear peak, with another smaller peak at 1.84ns far from the maximum value of the main peak
- **-1 :** Describes a clear peak, with another smaller peak at -1.84ns far from the maximum value of the main peak
- **2 :** Describes a clear peak, with another smaller peak at 2x1.84ns far from the maximum value of the main peak
- **-2 :** Describes a clear peak, with another smaller peak at 2x(-1.84)ns far from the maximum value of the main peak
- **1.1 :** Describes a clear peak, with another smaller peak at 1.84ns far from the maximum value of the main peak, with some additional entries which are not in a range of 0.25ns around the maximum of the peaks
- **-1.1 :** Describes a clear peak, with another smaller peak at -1.84ns far from the maximum value of the main peak, with some additional entries which are not in a range of 0.25ns around the maximum of the peaks
- **100 :** The histogram contains positive values. This category is existing because positive values are not expected and increase considerably the standard deviation of the distribution.
- **1000 :** The maximum of the main peak is greater than -4.5ns, which is expected as too high.

TABLE 1: *Percentages of channel offset histograms classified per category and boards.*

Cat.	B1	B2	B3	B4	B5	B6	B7	B8	B9	B10	B11	B12
0	38.7	47.7	67.8	43.2	55.5	27.9	30.5	37.109	36.5	42.8	36.3	55.9
0.1	52.9	36.5	31.4	47.7	42.2	59.0	50.4	56.3	53.3	45.9	51.4	34.4
1	0	3.7	0	2.5	0.8	6.3	0	0	0	0	0.8	3.1
-1	6.1	4.1	0.2	3.7	0	2.5	11.9	0.4	7.2	7.6	2.0	1.4
2	0	0	0	0	0	0	0.2	0	0	0	0	0
-2	0	0	0.2	0.2	0	0	0	0	0	0	0	0
1.1	0.6	2.1	0.2	0.4	1.4	3.9	0.2	1.0	0.4	0.4	7.2	4.7
-1.1	1.8	2.0	0.2	2.3	0.2	0.4	3.7	3.3	2.5	3.3	2.0	0.6
100	0	2.1	0	0	0	0	1.8	0	0	0	0	0
1000	0	1.8	0	0	0	0	1.4	2.0	0	0	0.4	0

5.2 Light propagation delay

As shown in figure 12, the position of a hit in the fibre mat has an impact on the light propagation time to the channel readout. In fact, a particle that arrives at channel 0 in a Y board has no light propagation delay, whereas in channel 511, the light has to propagate 133mm in the fibre. The light velocity in a scintillating fibre was measured to be (163 ± 3) mm/ns, which means that on a distance of 133mm, a delay of (816 ± 15) ps is induced. This value is non negligible to the expected time resolution of a few hundreds of ps. Therefore, this delay has to be compensated.

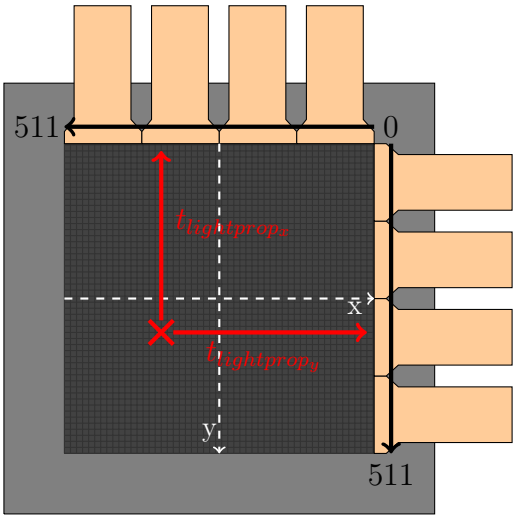

FIGURE 12: *Fibre mat in black, with the SiPMs reading out the signal given by the particle crossing the mat at the position of the red cross*

In order to take the light propagation delay into account, it has to be measured for each hit and cluster in the board. The centre of the fibre mat is the origin (0,0). The hit position x or y is then used to calculate the remaining distance to the SiPMs d by eq.(1).

$$\begin{cases} X \text{ Plane :} & 70 - y \\ Y \text{ Plane :} & 70 + x \end{cases} \tag{1}$$

The different calculation in both planes in eq.(1) is due to the fact that in the upper right corner of the fibre mat (see figure 12), is situated the point channel 0 in X and in Y, but in terms of position, it is at (+70, -70). The light propagation delay is then obtained for each event and hit by $t_{lightProp_{delay}} = \frac{d}{c_{fibre}}$, where d is the remaining distance from the hit to the SiPM and c_{fibre} is the measured velocity of the light in the scintillating fibre.

For run 1213, the light propagation delays in the X and Y planes are reported in the histograms of the figure 13. The position of the beam for run 1213 is at (-30, +30)mm, which means that the beam is in the lower left corner of the fibre mat. The distance for the photons to the SiPMs is therefore approximately the same for the x direction as for the y direction. Those plots can also be interpreted as beam profiles in time.

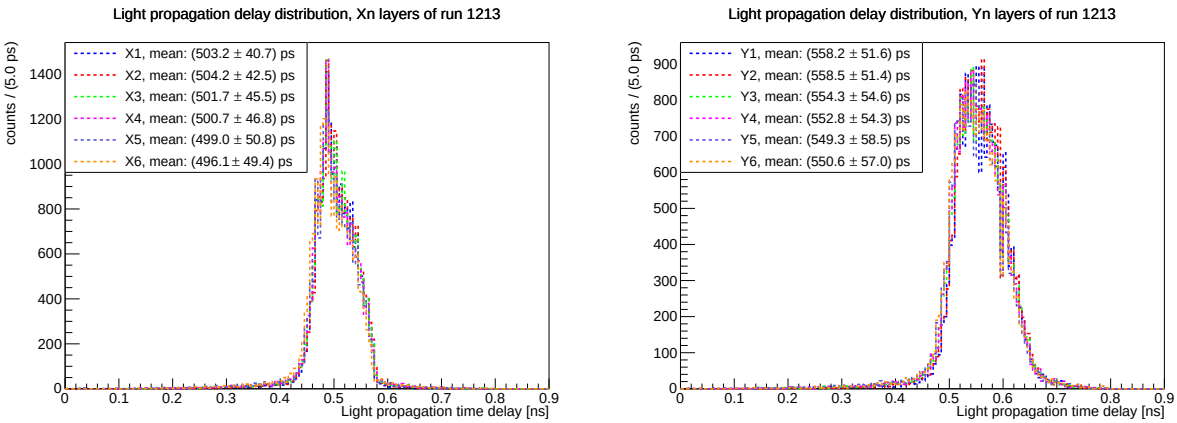

FIGURE 13: *Light propagation delay for the run 1213. On the right hand-side: in the X planes and on the left hand-side: in the Y planes.*

5.3 Board fine time offsets

The board offset correction is in the order of several hundreds ns of magnitude. Due to the fact that a time resolution of a few hundreds ps is expected, this time offset can be improved by including a fine board time offset.

In order to measure the fine time board offset, the events are chosen such that they have only one cluster per board. The time of the cluster is defined by the fastest hit in the cluster, and it is computed in each board. The time difference $t_{b_i} - t_{b_j}$ can be computed, where t_{b_i} and t_{b_j} are respectively the cluster times in board i and j. Computing this value for each of the events, a histogram can be obtained for each of the pair of boards used. For simplicity, the board Y1 is taken as reference for the Y planes and X1 for the X planes. The distribution is then fitted by a Gaussian curve to obtain a precise mean and standard deviation of the histogram. In figure 14, the histograms of the time difference of run 1213, for board Y1 and Y2, and X1 and X2, including the previously mentioned offsets, are shown. The time difference between the other boards taking X1 and Y1 as reference for run 1213 are shown in the appendix C. The standard deviation of the fitted distribution is called the Coincidence Time Resolution (CTR), and is a strong indication on the time resolution of the detector.

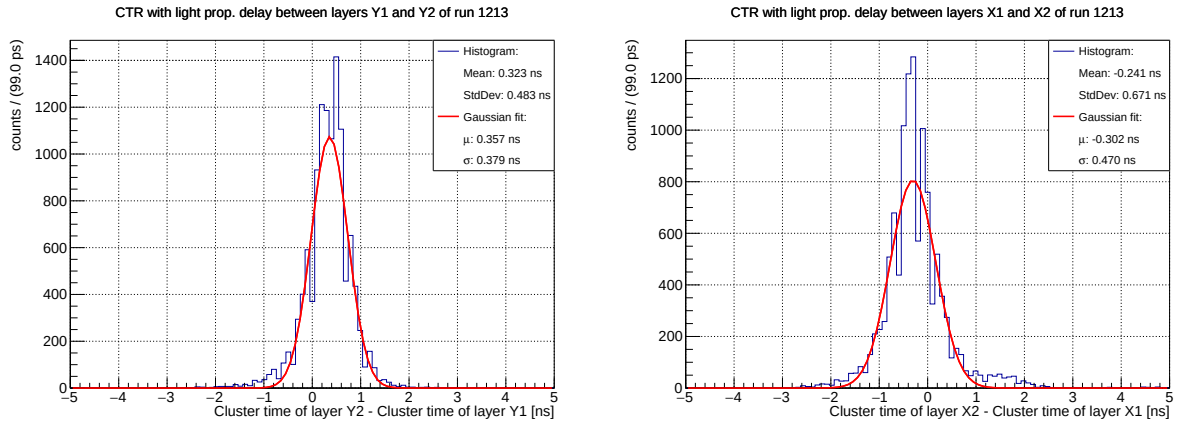

FIGURE 14: *The Cluster Time difference distribution between boards, Y1 and Y2 on the left, X1 and X2 on the right, in blue and its Gaussian fit in red.*

The mean of the fitted distribution on figure 14, reads the board fine time offset. This value can

be improved using an iterative process. The value obtained is subtracted as a time offset from the cluster time, and the remaining mean value of the CTR is added to the fine board time offset obtained in the previous step. This is repeated until the mean of the fitted CTR reaches a value of 10^{-5}ns. The final fine board time offsets are reported in table 2. It is noticeable that for each board the obtained offsets are in the same order of magnitude for all the runs, except for run 1216, due to the fact that board X1 and Y4 where wrongly calibrated for this run.

TABLE 2: *The measured board time offsets for all the runs and the fine board time offsets for each studied run.*

	Board time offset [ns]	Run 1213 [ps]	Run 1214 [ps]	Run 1215 [ps]	Run 1216 [ps]
Y1	-172	0	0	0	0
X1	-212	0	0	0	0
Y2	-204	350	319	361	326
X2	-243	-294	-304	-443	6303
Y3	-168	489	451	470	473
X3	-207	-256	-261	-422	6288
Y4	-198	-597	-592	-563	-7179
X4	-239	-123	-114	-239	6580
Y5	-167	120	128	133	182
X5	-207	-324	-309	-524	6222
Y6	-199	495	498	520	548
X6	-238	-175	-174	-348	6379

5.4 Channel fine time offsets

The fine time correction of a channel can be extracted from the track time. Firstly, the characteristics of a track have to be defined, as well as its time. The requirements for a track consist of having exactly one cluster in each board and that their timestamps are in the same order of magnitude. An additional requirement is that the incident beam is quasi perpendicular to the board. This constrains the number of events that satisfy and contain a track definition.

The track time has to be defined and computed, with the available time variables the cluster times. In this project, four different algorithms have been developed, to have a comparison and establish the best working algorithm. The four definitions of the algorithms are given by the following:

- **1st algorithm:** The mean value of the cluster times of the boards $X1$, $X2$ and $X3$ are calculated.
- **2nd algorithm:** The mean value of the twelve cluster times of all the boards are computed.
- **3rd algorithm:** The mean value of the three smallest cluster times, the three fastest hits, is taken.
- **4th algorithm:** The mean value of a set of eight cluster times is taken, where the two fastest and the two slowest clusters are removed.

The cluster time is computed for each board and each event by applying the previously measured offsets. The four defined algorithms are applied and the track time is determined for each event.

In order to check if the algorithms are defining the track time correctly, the time residual is calculated in a similar way as in the section (5.3) for the CTR. The residual is computed by the relation $t_{track} - t_{b_i}$, where t_{track} is the track time computed above and t_{b_i} is the cluster time in the board i. In the section (5.3), a CTR of less than 350 ps has been determined. The standard deviation of the time residual is expected to be of the order of $350/\sqrt{2}$. The reducing of the σ is due to the usage of the track time and the fact that two quantities have the same σ. In figure 15, the distribution of $t_{track} - t_{b_i}$ is shown for run 1213 and board 7, where each of the distribution is fitted by a Gaussian distribution.

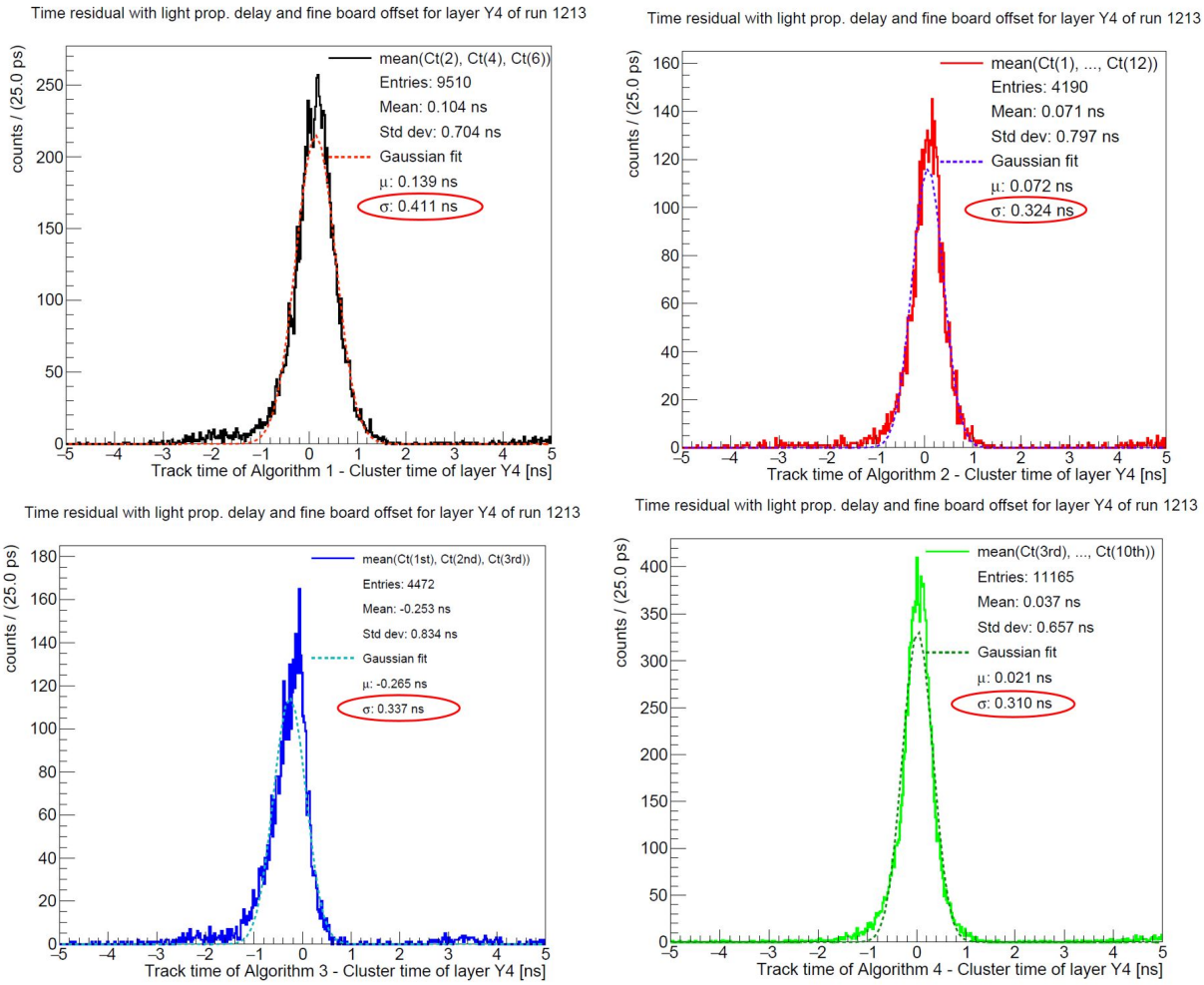

FIGURE 15: $t_{track} - t_{b_7}$ *distribution for run 1213, where* t_{b_7} *is the cluster time in board 7. From left to the right: algorithm 1, algorithm 2, algorithm 3 and algorithm 4.*

In figure 15, the distribution of the time residual is narrow and the σ is about 350ps for all the algorithms or even less. Also, the rising edge (located on the right) is steep, which means that there are not many entries of cluster times arriving early compared to the track time. However, on the falling edge (located on the left), there are more hits coming later than the track time. Also, most evidently in the distribution of algorithm 1, a small bump is appearing at $\sim$ -1.84ns, which originates from the STiC chip bug. In the end, this crosscheck demonstrates that the algorithms are describing well the track time. The 4th algorithm has the sharpest peak, which means the lowest value of σ for the fit, and will therefore be used in the further analysis.

In order to determine the channel fine time offset, the time residual is calculated using channel information, not boards one as previously. The time residual is now defined as $t_{track} - t_{hit}$, where t_{hit} is the time of the hit in the board. The shape of such a distribution is shown as

example in the figure 16 for run 1214, board 6 and channel 366, where the distribution is fitted by a Gaussian distribution.

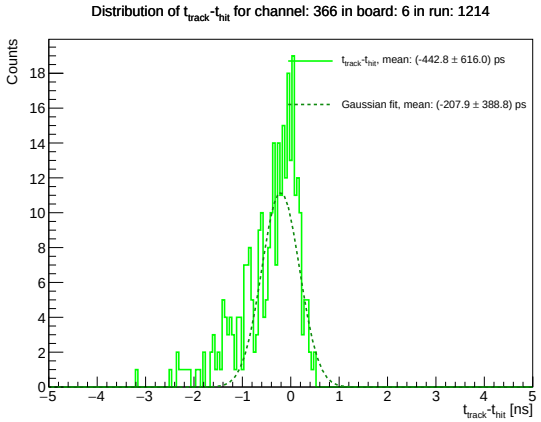

FIGURE 16: *$t_{track} - t_{hit}$ distribution for run 1213, board 6 and channel 366, fitted by a Gaussian distribution.*

The analysis of the shape of the distribution in figure 16 is similar to the one of the previous residual, however in this case there are more entries at negative values. This is due to the fact that there are more hits arriving late, because the neighbouring channels are taken into account. In those channels, the number of produced photons in the fibre is lower than in the central one and have a longer propagation to the SiPMs. Therefore, also the σ from the fit is larger due to that reason. The mean of the fitted distribution is therefore the channel fine time correction. However, to avoid having random corrections, it is required that such a distribution has at least 100 entries and that the mean of the fit is less than 5ns.

The channel fine time correction is applied on the cluster time computation and the time residual $t_{track} - t_{b_n}$ distribution is plotted again. In figure 17, on the left graph, the corrected residual is shown for board 7 and run 1213 for the fourth algorithm, and in the right graph, a summary of the σ of the fit of the distribution for all boards of this run is shown.

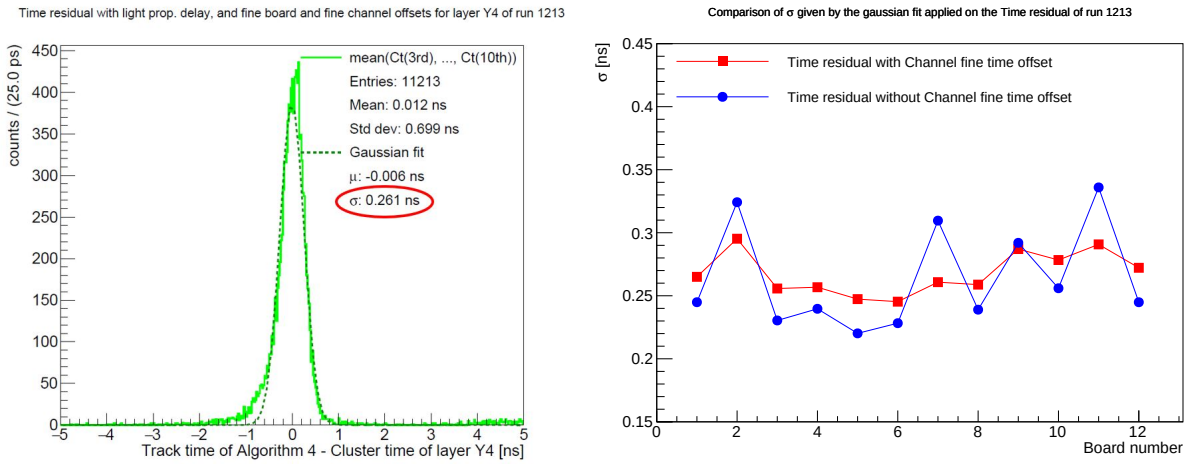

FIGURE 17: *On the left hand-side: $t_{track} - t_{b_7}$ distribution, where t_{b_7} is the cluster time in board 7, with the channel fine time correction applied. On the right hand-side, the σ of the fit of the time residual distribution for all the boards with and without the fine time correction for the run 1213.*

Before the correction, the σ of the time residual was 310ps for the board 7 in run 1213 (see

figure 15) and after the fine channel time correction, the left graph of figure 17 shows a σ of 261ps. The right graph of figure 18 shows the standard deviation of the time residual before and after the fine channel time correction for all the boards. For the outlaying points, the correction works well, however, for the boards that had already a good time residual before the correction, their values are slightly increased. It seems that the red curve smooths and adapts the values that can not be improved to the others, by rising the lower ones. The summary of the σ of the fitted residual distribution for the other runs are shown in the figure 18.

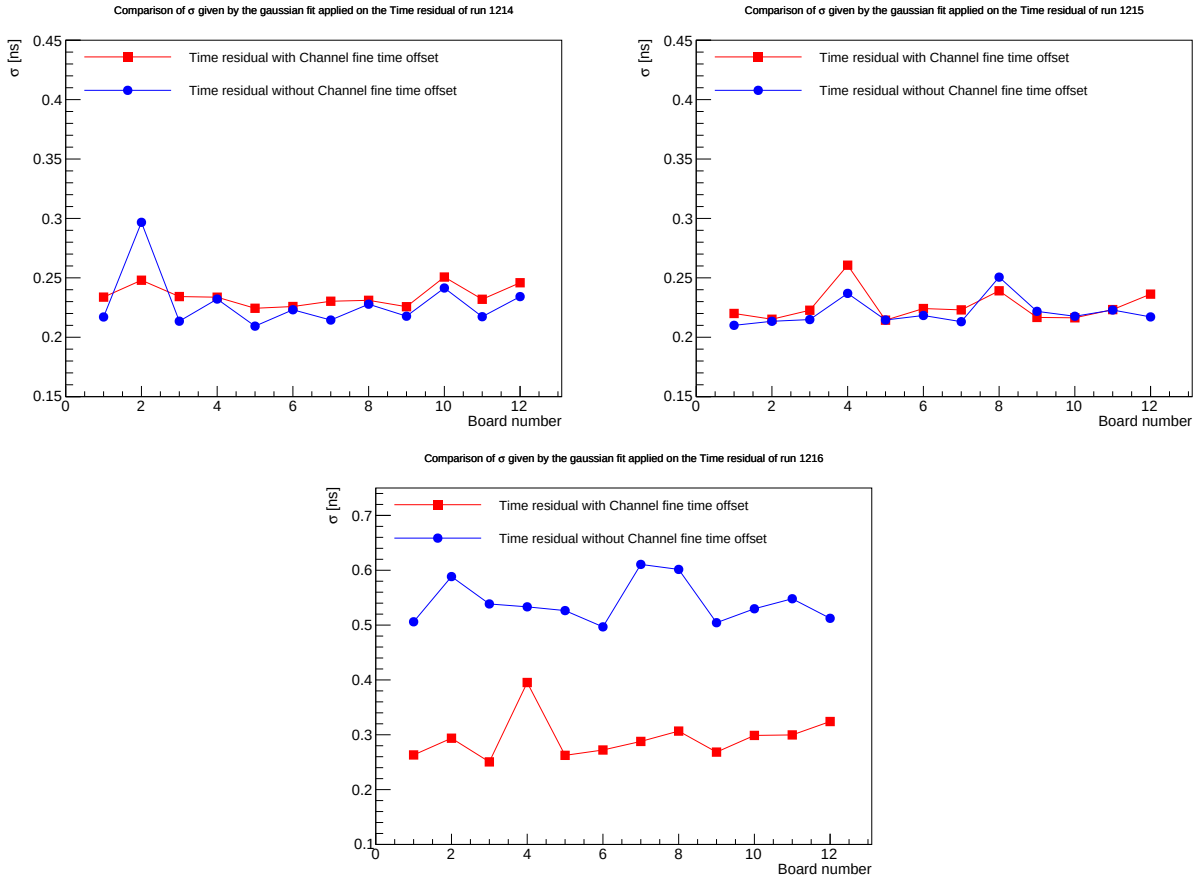

FIGURE 18: *The σ of the fit of the time residual distribution for all the boards with and without the fine time correction for the runs 1214, 1215 and 1216.*

A general conclusion for the channel fine time correction is that the σ of the fitted residual distribution is smoothed in all the boards and the mean time residual is improved from the previous result, without the channel fine time correction. In particular for run 1216, the improvement is great, due to the fact that this run has been wrongly calibrated before the data taking. The channel fine time correction recovered these problems and shows a residual which is considerably improved. Finally, the channel fine time correction does not impact much the runs that were correctly calibrated before, however, it recovers the previous errors and gives a satisfying residual in the end.

5.5 Verification of the algorithm

To ensure the implementation of the algorithm works correctly, two checks are performed. Run 1214 (which has been correctly calibrated) is chosen to add some artificial errors in the calibration files of board 6 such that the previous calibration is not correct anymore. The algorithm should be able to correct these induced errors and the same final result should be obtained.

The first check consists of adding 200ps to all the channel offsets of board 6 in run 1214. This additional time should be recovered in the board fine time offsets, due to the fact that it is the same in all the channels. The obtained results are shown in figure 19, which are in agreement with the predictions. In fact, the board fine time offset of board 6(X3) is 200ps lower as in the analysis (see table 2), which shows the compensation of the induced artificial error in this step, and for the time residual standard deviations, values remain unchanged.

	Run 1214 [ps]
Y1	0
X1	0
Y2	319
X2	-304
Y3	451
X3	-461
Y4	-592
X4	-114
Y5	128
X5	-309
Y6	498
X6	-174

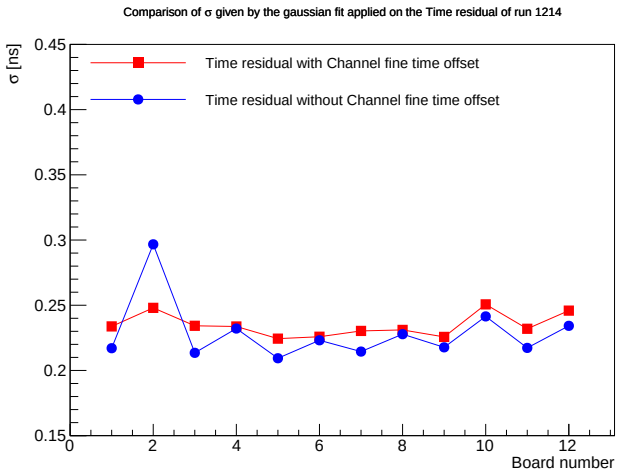

FIGURE 19: *On the left: the measured board fine time offsets for run 1214, by adding 200ps to each channel offset in board 6. On the right: the σ of the residual before and after the channel fine time correction.*

A second check is done, which consists of adding 200ps to all odd channels of board 6 of run 1214 and subtracting 200ps on all the even channels. This should not be recovered by the board fine time offsets, because not all the channels have the same error. The time residual without the channel fine time correction is therefore expected modified from the result of the blue curve of figure 18, but the applied channel fine time correction should recover this error and result in the similar values as the red curve in figure 18. The obtained results applying this artificial error are shown in figure 20. The board fine time offset of the board 6(X3) is equal to -297ps, which is in the same order of magnitude as -261ps, which was the value in the analysis (see table 2). However the residual without the channel fine time correction for board 6 is higher than in the analysis (see figure 18). The channel fine time offset recovers this peak in board 6 and its residual has in the end the same value than in the analysis. Those results are also in agreement with the predictions and confirm the accuracy of the algorithm.

	Run 1214 [ps]
Y1	0
X1	0
Y2	319
X2	-304
Y3	451
X3	-297
Y4	-592
X4	-114
Y5	128
X5	-309
Y6	498
X6	-174

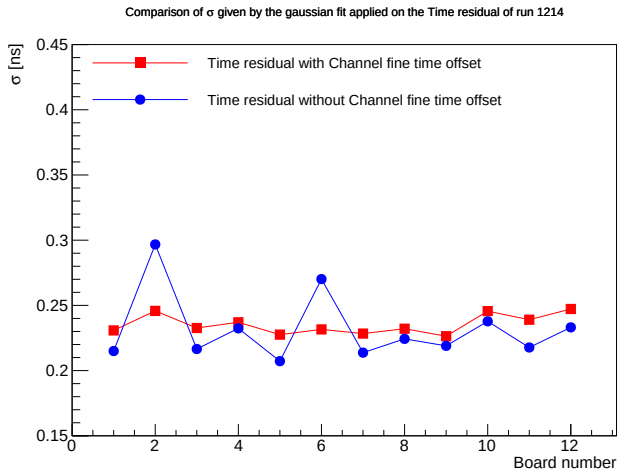

FIGURE 20: *On the left: the measured board fine time offsets for run 1214, by adding 200ps to all odd channel offsets and subtracting 200ps to all even channels offsets in board 6. On the right: the σ of the residual before and after the channel fine time correction.*

6 Summary and conclusion

The analysis of the time resolution of the SciFi tracker with the DESY data from the testbeam, gives information about the previous calibration of the detector, indications to improve it and finally quantifies the different offsets and delays.

Previously measured channel offsets have been analysed for all runs, and allow to get a first indication of the accuracy of the correction. The mean value provides information of the accuracy of the calibration runs. They show that the quality of the calibration is not always sufficient. Four runs that show a good calibration are chosen for further analysis.

The light propagation delay of the photons created by the distance between the hit position and the SiPM is an important delay that has to be taken into account for the cluster time calculation. The combination of the x and y position allows to determine this delay and verify that they correspond to the beam profile in time.

Then the board offset can be improved. A precise board offset is needed to calculate the track time. It has been previously calibrated with a trigger system, but the measurement of the offsets is not precise enough. The cluster time is computed in each of the boards and taking Y1 as reference for the Y planes and X1 for the X planes, the difference can be measured, and improved by repeating the procedure several times.

Finally, the channel fine time offset is measured using the track information. The track time is defined with four different algorithms for comparison, and the most promising one (Algorithm 4, see p.13) is chosen. This algorithm is then used to compute the channel fine time offset taking the mean of the fitted distributions of $t_{track} - t_{hit}$. Applying the measured correction to the time residual, the improvements are clearly visible for the boards, with a bad calibration, however, for the well calibrated boards, the improvement is negligible. The σ of the fitted residual curve is smoothed and the mean is improved. The SciFi tracker in the configuration with short fibre mats (133mm) and 7 fibre layers can reach a time resolution over the full plane of 200ps. The amount of light, the electronics, the scintillator decay time, as well as the delay in the fibre propagation are all factors that are limiting the detector's resolution.

The verification of the algorithm demonstrated that using the track information, errors in previous measured time offsets can be recovered. This result shows that using the track properties to compute the time offsets, no previous calibration is needed. The prove of this concept is an important milestone for the future implementation of the time calibration of the SND@LHC detector. In fact, using the track information would be a perfect way for the time calibration of the detector, making use of the muon tracks. This will simplify considerably the data taking, due to the fact that the detector is not accessible during the run time of the LHC.

Acknowledgements

I would like to express my gratitude to Dr. Guido Haefeli, Dr. Ana Barbara Rodrigues Cavalcante and the Doctoral Assistant Carina Trippl for their continuous support throughout this work and for sharing their knowledge and experience in particle physics and in detector technology.

I finally would like to thank Prof. Dr. Olivier Schneider for making that project possible.

A Run selection extract

TABLE 3: *Extract of the qualification of the runs per board, where the number of the event indicates that it satisfies the requirements, "-00-" and "-28-" stand for dead channels, and finally "- - - -" indicates that there is no corresponding calibration file.*

B1	B2	B3	B4	B5	B6	B7	B8	B9	B10	B11	B12
-28-	-28-	-28-	-28-	-28-	-28-	-28-	-28-	-28-	-28-	-28-	-28-
- - - -	- - - -	- - - -	- - - -	- - - -	- - - -	- - - -	- - - -	- - - -	- - - -	- - - -	- - - -
-28-	-28-	-28-	-28-	-28-	-28-	-28-	-28-	-28-	-28-	-28-	-28-
1011	1011	1011	1011	1011	1011	1011	1011	1011	1011	1011	1011
-28-	-28-	-28-	-28-	-28-	-28-	-28-	-28-	-28-	-28-	-28-	-28-
1021	1021	1021	1021	1021	1021	1021	1021	1021	1021	1021	1021
...	...	...	...	...	...	...	...	...	...	...	...

B Figures for the channel offsets

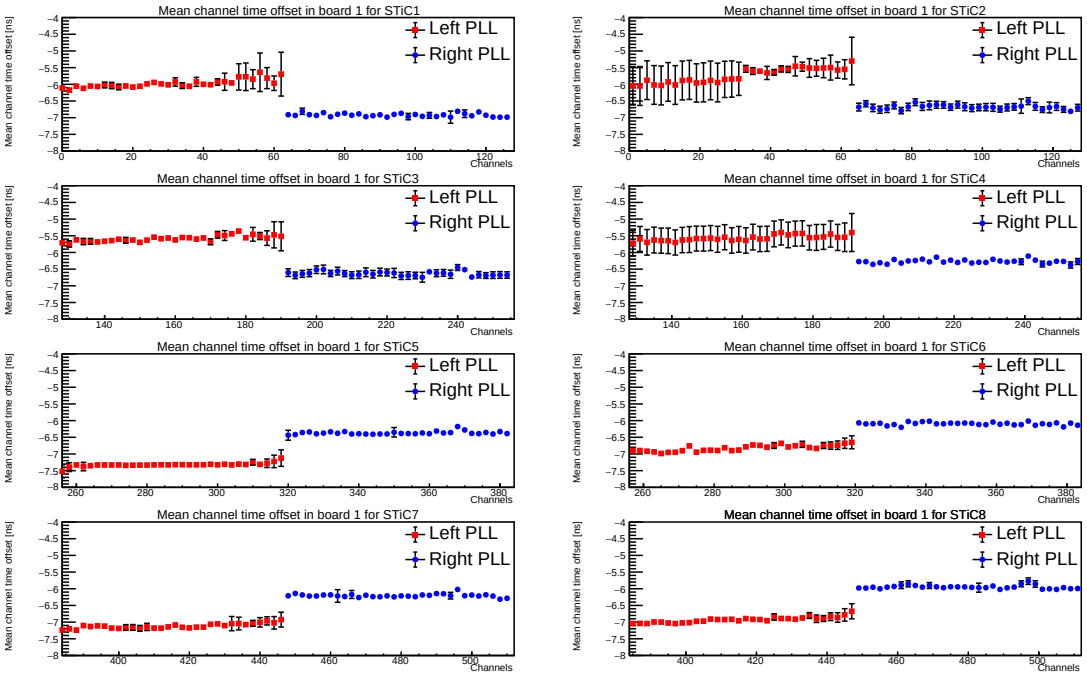

FIGURE 21: *Channel offsets per STiC and PLL in board 1.*

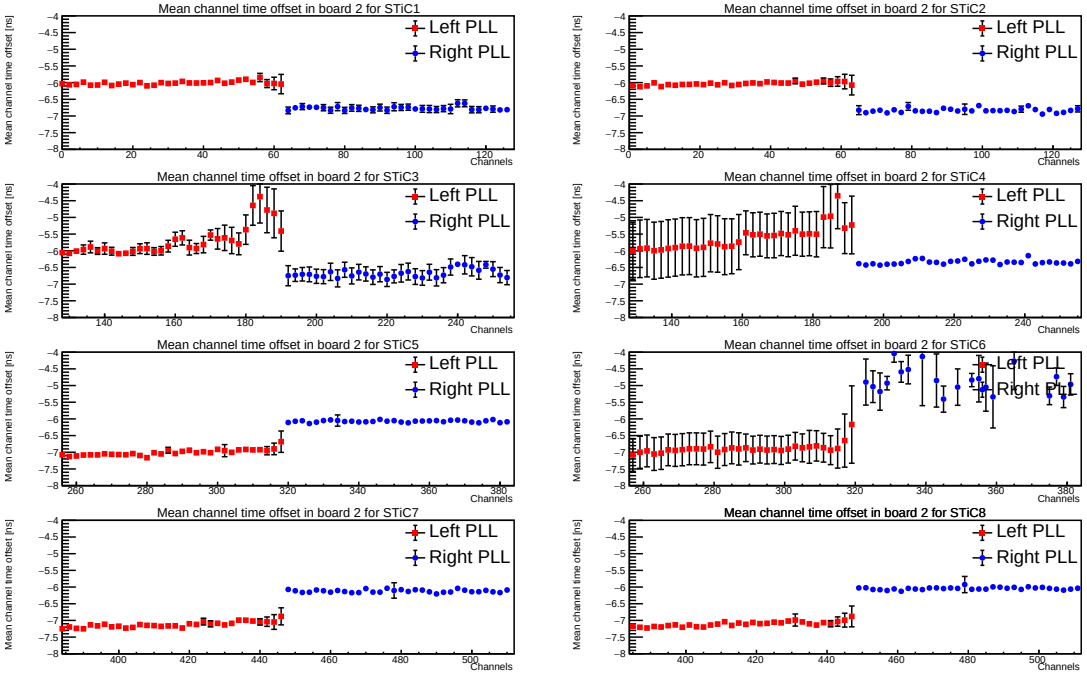

FIGURE 22: *Channel offsets per STiC and PLL in board 2.*

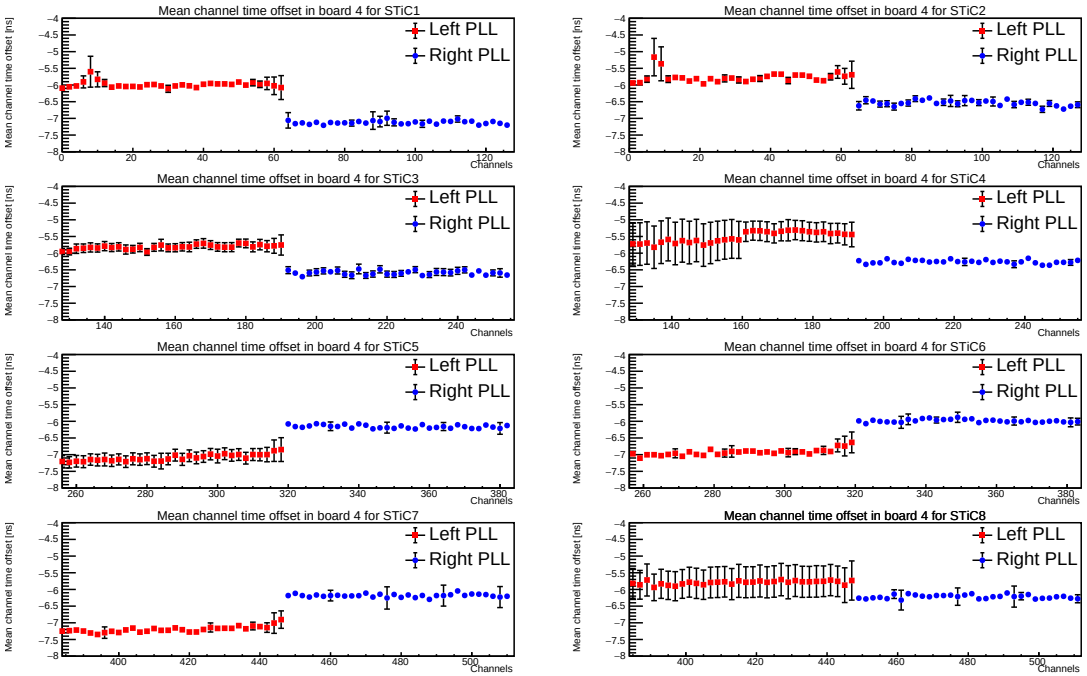

FIGURE 23: *Channel offsets per STiC and PLL in board 4.*

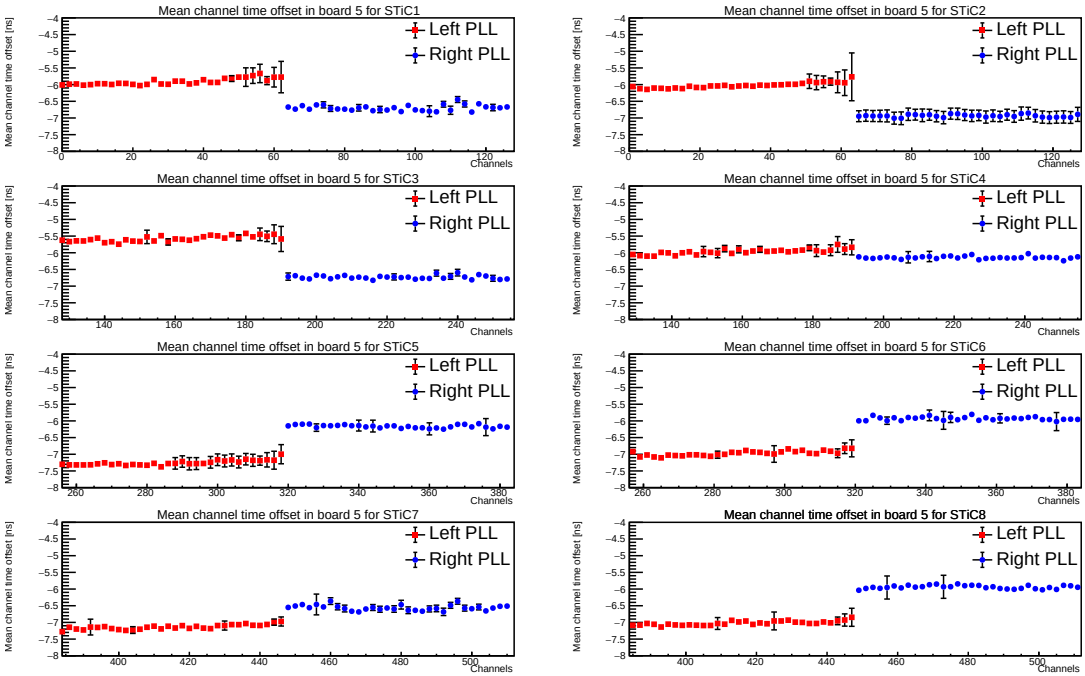

FIGURE 24: *Channel offsets per STiC and PLL in board 5.*

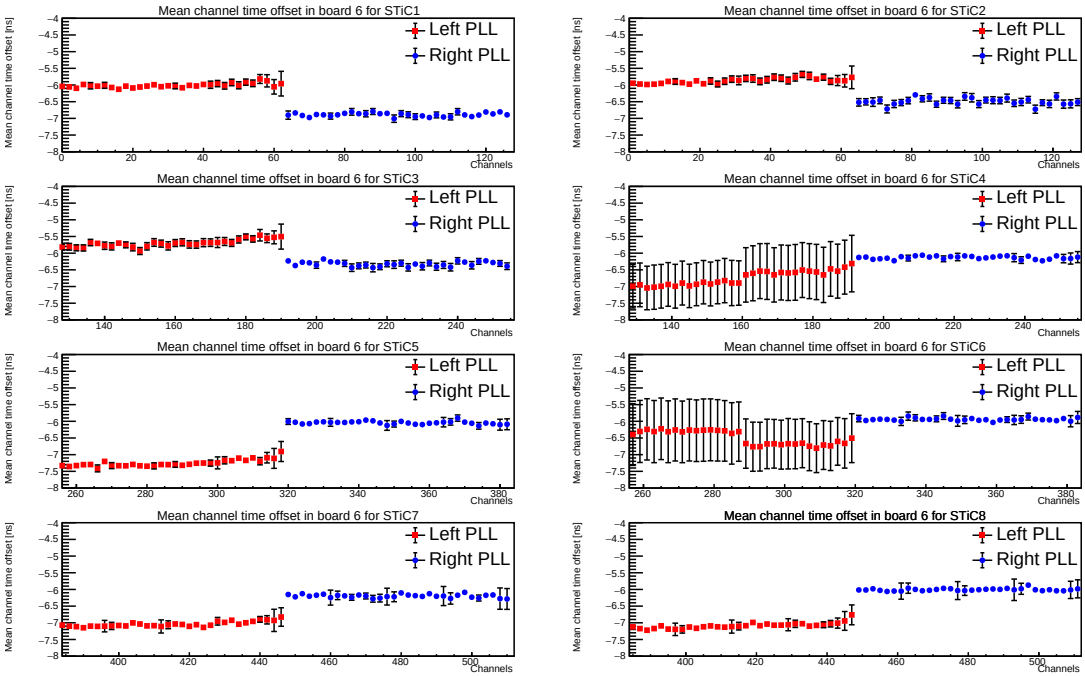

FIGURE 25: *Channel offsets per STiC and PLL in board 6.*

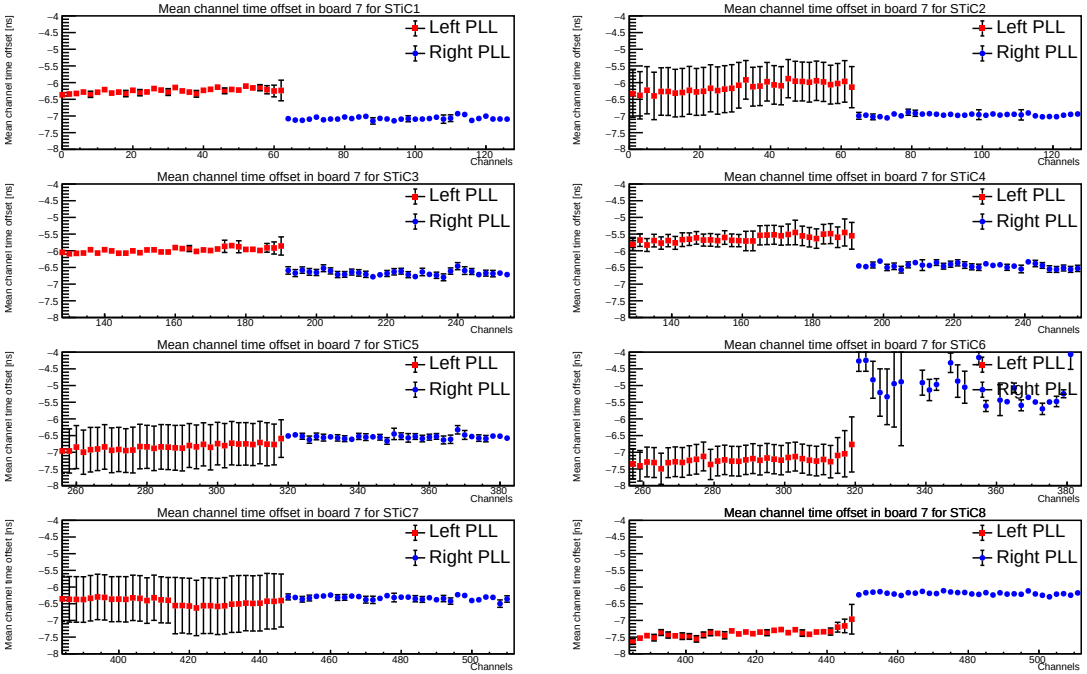

FIGURE 26: *Channel offsets per STiC and PLL in board 7.*

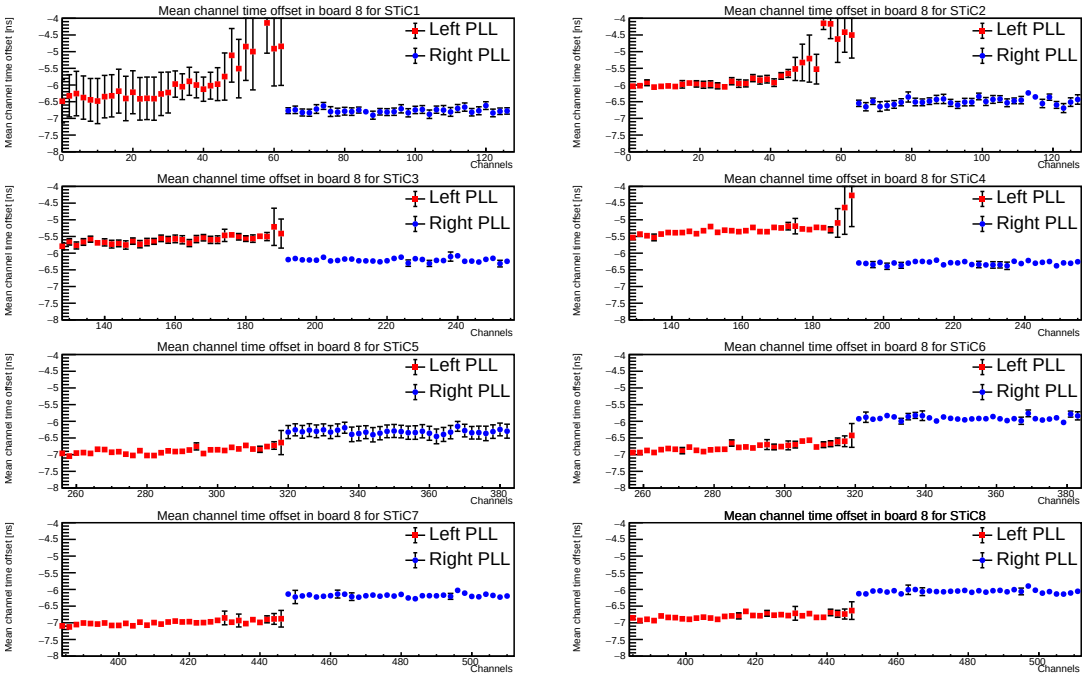

FIGURE 27: *Channel offsets per STiC and PLL in board 8.*

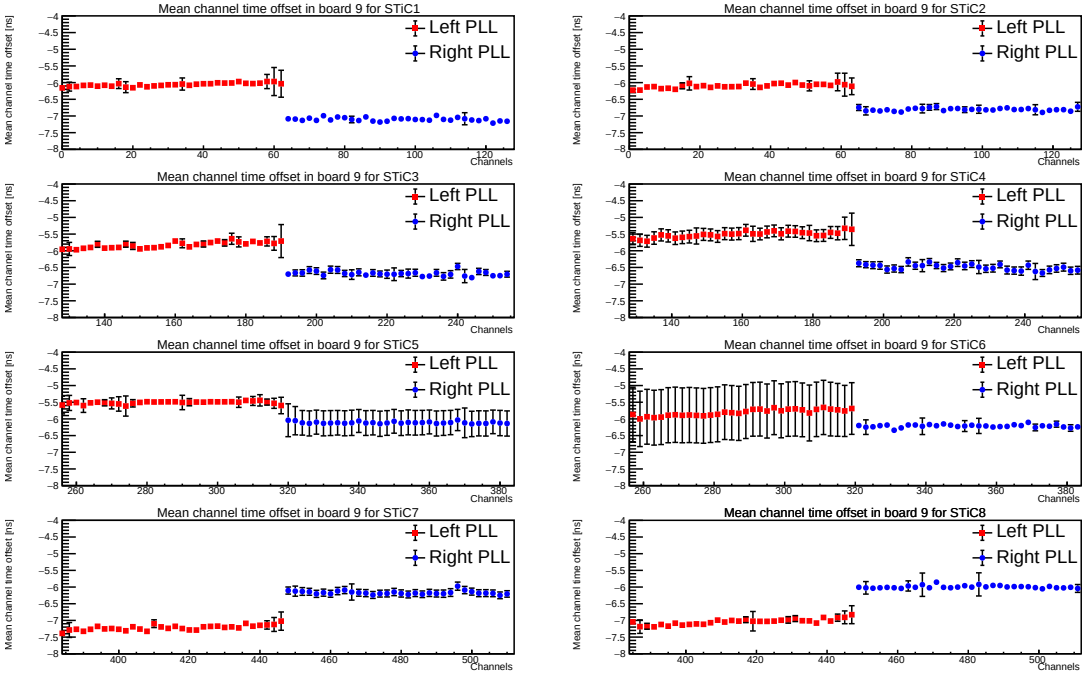

FIGURE 28: *Channel offsets per STiC and PLL in board 9.*

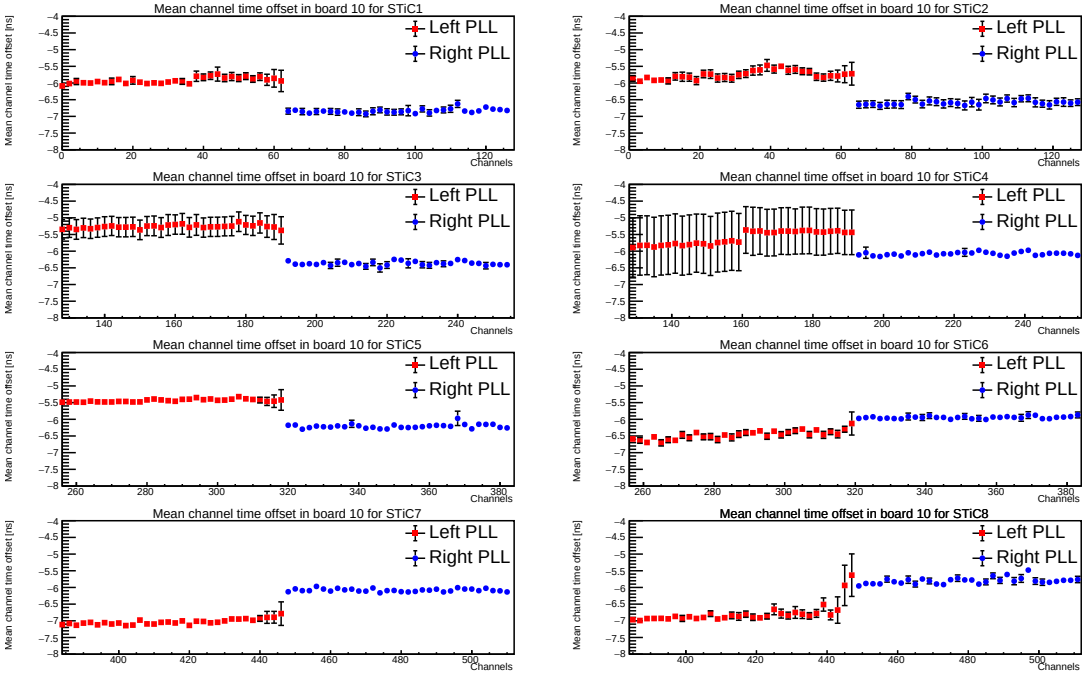

FIGURE 29: *Channel offsets per STiC and PLL in board 10.*

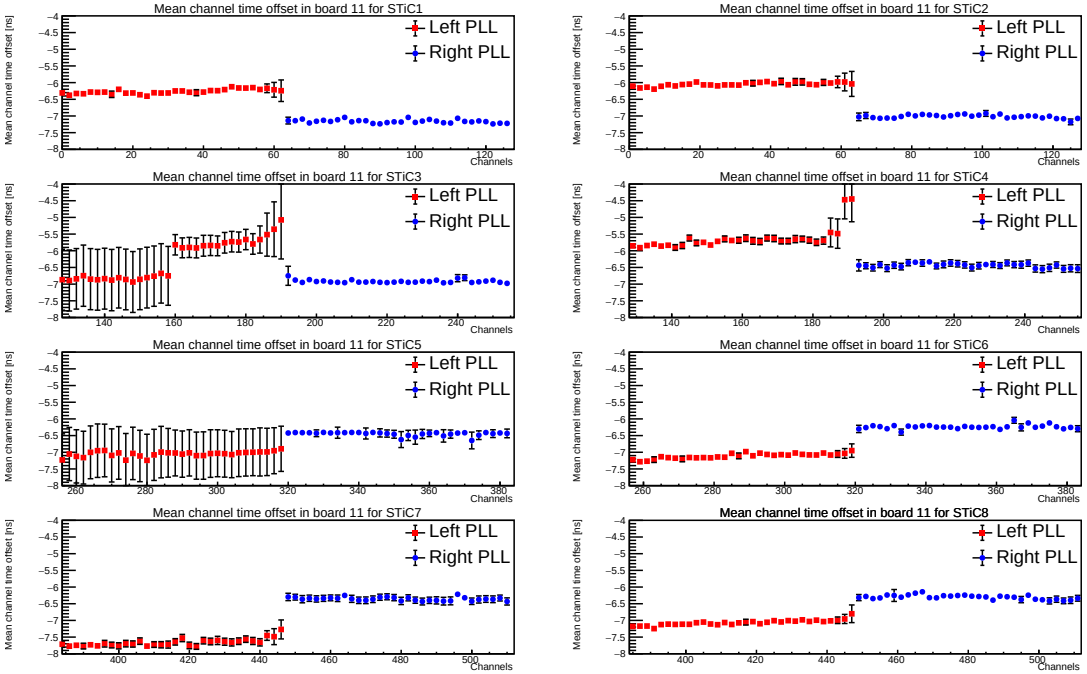

FIGURE 30: *Channel offsets per STiC and PLL in board 11.*

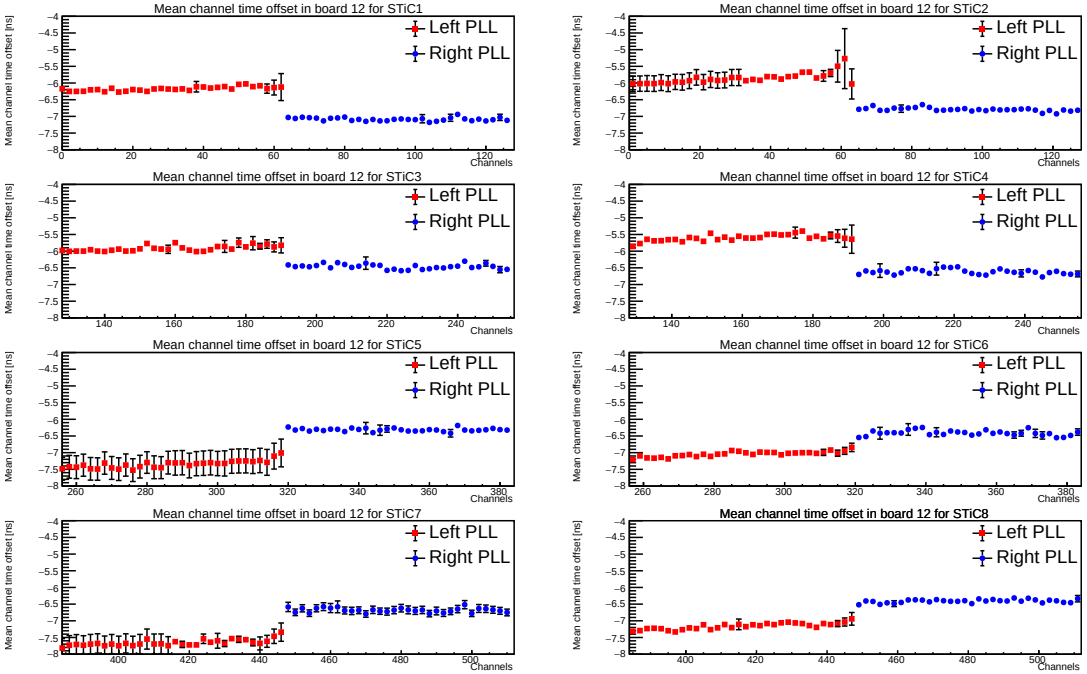

FIGURE 31: *Channel offsets per STiC and PLL in board 12.*

C Cluster Time difference distributions for run 1213

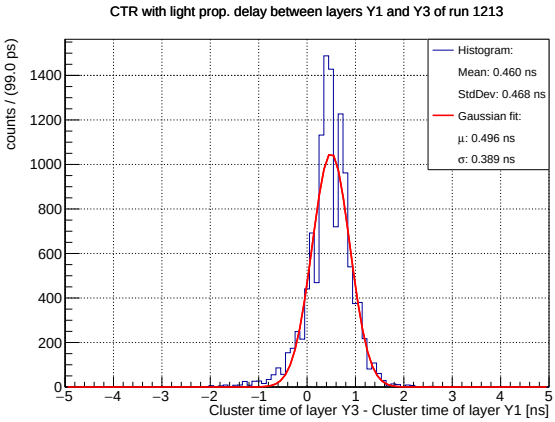

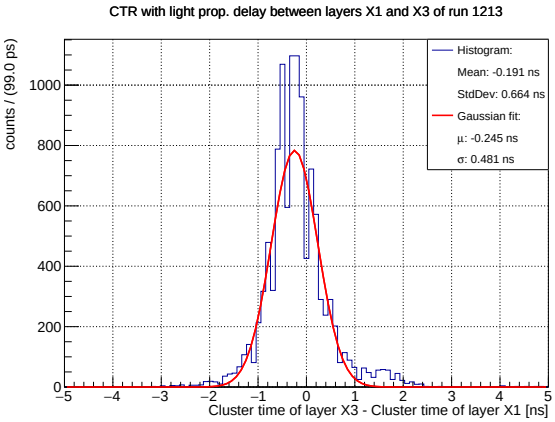

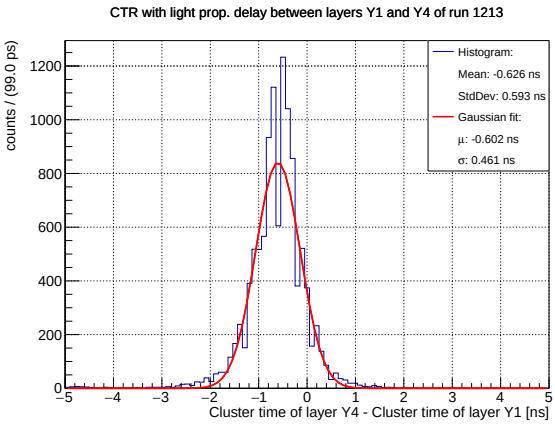

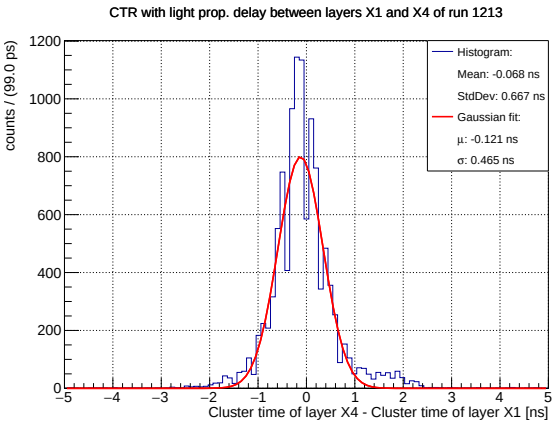

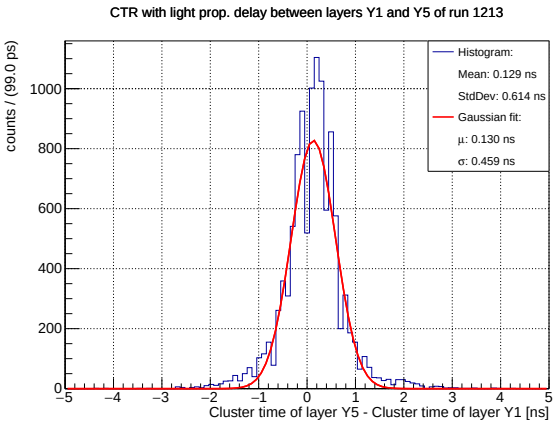

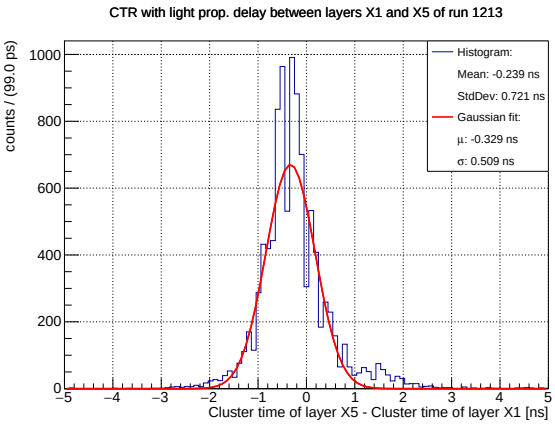

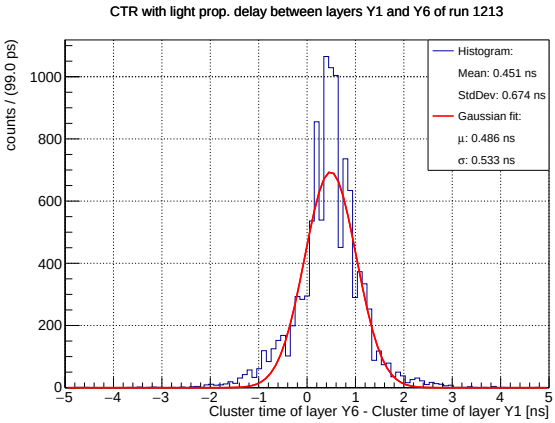
CTR with light prop. delay between layers Y1 and Y6 of run 1213
counts / (99.0 ps)
Cluster time of layer Y6 - Cluster time of layer Y1 [ns]
Histogram:
Mean: 0.451 ns
StdDev: 0.674 ns
Gaussian fit:
μ: 0.486 ns
σ: 0.533 ns

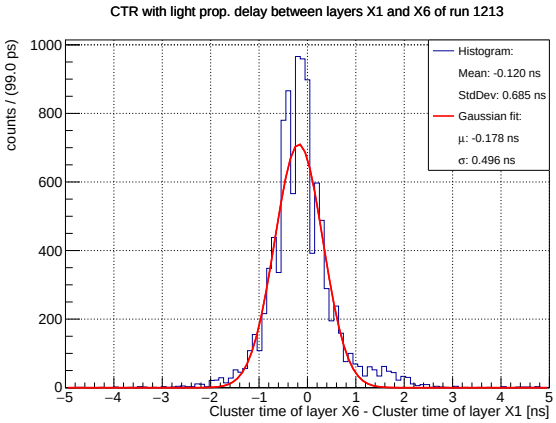
CTR with light prop. delay between layers X1 and X6 of run 1213
counts / (99.0 ps)
Cluster time of layer X6 - Cluster time of layer X1 [ns]
Histogram:
Mean: -0.120 ns
StdDev: 0.685 ns
Gaussian fit:
μ: -0.178 ns
σ: 0.496 ns

References

[1] The SHiP Collaboration, 21 February 2020: *SND@LHC* [Consulted in April 2020] Available on: https://arxiv.org/pdf/2002.08722.pdf

[2] HAEFELI Guido, November 2019: *SciFi timing tracker, R&D status* [Consulted in April 2020]

[3] LHCB, 7 february 2020: *TestbeamOct2019@DESY* [Consulted in April 2020] Available on: https://twiki.cern.ch/twiki/bin/view/LHCb/TestbeamOct2019

[4] MASCELLANI Anna, fall Semester 2019: *Studies on a SciFi Tracker with Cosmic Rays and Test Beam Data* [Consulted in April 2020]

[5] KUONEN Axel, 21 september 2018: *Development and Characterisation of Silicon Photomultiplier Multichannel Arrays for the Readout of a Large Scale Scintillating Fibre Tracker* [Consulted in April 2020] Available on: https://www.epfl.ch/labs/lphe/en/publication/

[6] HARTMANN Marco, 11 November 2019: *Study of a Scintillating Fibre Tracker using DESY testbeam data* [Consulted in April 2020]